Electroweak pion production on nuclei within the extended factorization scheme

Noemi Rocco,[1,2] Satoshi X. Nakamura,[3,4] T.-S. H. Lee ●,[1] and Alessandro Lovato ●[1,5]

[1]*Physics Division, Argonne National Laboratory, Argonne, Illinois 60439, USA*
[2]*Theoretical Physics Department, Fermi National Accelerator Laboratory, P.O. Box 500, Batavia, Illinois 60510, USA*
[3]*Department of Modern Physics, University of Science and Technology of China, Hefei 230026, People's Republic of China*
[4]*State Key Laboratory of Particle Detection and Electronics (IHEP-USTC), Hefei 230036, People's Republic of China*
[5]*INFN-TIFPA Trento Institute of Fundamental Physics and Applications, Via Sommarive, 14, 38123 Trento, Italy*

We have applied the extended factorization scheme to investigate the electroweak pion production on nuclei. The ANL-Osaka model, which was obtained by analyzing the data of πN, γN, $N(e, e'\pi)$, and $N(\nu, \mu\pi)$ reactions up to invariant mass $W = 2$ GeV, is used to generate the matrix elements of current operators relevant to pion production off the nucleon. Medium effects on the $\Delta(1232)$ component of the meson-exchange current are included by using a Δ-nucleus potential determined from the previous Δ-hole model studies of pion-nucleus reactions. Nuclear correlations in the initial target state and in the spectator system(s) are modeled using realistic hole spectral functions. As a first step, we show that the data of ^{12}C(e, e') up to the $\Delta(1232)$ region can be described reasonably well. The interplay between the pion production and two-body meson-exchange mechanisms is shown to be essential in improving the agreement with the data in the "dip" region, between the quasielastic and the $\Delta(1232)$ peaks. Predictions for ^{12}C$(\nu, \mu\pi)$ have also been made. They can be used to estimate pion-emission rates in neutrino-nucleus cross section, which constitutes an important systematic uncertainty to the reconstructed neutrino energy. With further improvements of the Metropolis Monte Carlo techniques to account for final states comprised of more than two particles, our approach can be employed up to $W = 2$ GeV, where two-pion production and higher mass nucleon resonances must be included for analyzing the data from accelerator-based neutrino-oscillation experiments.

I. INTRODUCTION

The development of the worldwide accelerator-based neutrino-oscillation program has been a springboard for advancing the theoretical description of lepton interactions with nuclei [1–3]. Oversimplified models of nuclear dynamics, such as the relativistic Fermi gas, have proven to be inadequate to reproduce quasielastic charge-changing scattering data on ^{12}C [4,5]. As a result, more sophisticated approaches, capable of providing a rather accurate description of available inclusive neutrino scattering data, have been devised [6–14]. In particular, the Green's function Monte Carlo (GFMC) method [15] has been successfully applied to perform *first principle* calculations of the neutral-current response functions in the quasielastic (QE) region, up to moderate values of the momentum transfer [16,17]. GFMC results have unambiguously identified the role of nuclear correlations and meson-exchange currents in providing the most accurate description of lepton-nucleus scattering. Although QE processes dominate the total cross section for neutrino fluxes in the sub-GeV region, as in T2K [18] and MicroBooNE [19] experiments, pion production constitutes an important background. A signal corresponding to a pion produced in the primary vertex and later absorbed in the nucleus could be misidentified with a QE event. Accurate predictions for inelastic channels are fundamental for experiments characterized by higher neutrino energies, such as MINERνA [20], NOνA

[21], and DUNE [22]. Extending the applicability of GFMC to processes with energies higher than those corresponding to the QE kinematics poses nontrivial difficulties. The use of integral-transform techniques precludes a proper treatment of the energy dependence of the current operators. In addition, despite strategies to include the leading relativistic effects in the kinematics exist, the explicit inclusion of pions, needed for a proper description of the resonance region, is still in its infancy [23].

The framework based on the impulse approximation (IA) and realistic hole spectral-functions (SFs) is ideally suited to combine a realistic description of the initial target state—as in the GFMC a realistic phenomenological Hamiltonian is employed—with a fully relativistic interaction vertex and kinematics [24]. In its original formulation, this factorization scheme relies on the assumption that lepton-nucleus scattering reduces to the incoherent sum of elementary processes involving individual nucleons. Over the past few years, the IA was generalized to include the excitation of two-particle–two-hole final states induced by relativistic meson-exchange currents [25]. This extended factorization scheme (EFS) has been applied to calculate the electroweak inclusive cross sections of carbon and oxygen [26,27].

Early investigations of real-pion emission in inclusive ^{12}C(e, e') scattering were carried out within the IA in Refs. [28–30]. There, the elementary $\gamma^* N \to \pi N$ cross

sections, generated from tree-diagram models consisting of the standard Born terms and the excitation of the $\Delta(1232)$ resonance, were convolved with the nucleon momentum distributions. The two-nucleon mechanism $\gamma^* + NN \rightarrow \Delta N \rightarrow NN$ was included [30] with the parameters determined by fitting the total cross section data of $\gamma + d \rightarrow np$ reaction in the Δ excitation region. Medium effects on the Δ propagation, mainly due to the pion absorption within the nucleus [31] were modeled using a Δ-nucleus potential, which was phenomenologically determined within the isobar-hole model of π-nucleus scattering [32–34]. The authors of Ref. [35] improved upon the above procedure by considering the $\gamma^* N \rightarrow \pi N$ amplitudes generated from a dynamical model [36,37], known as the Sato-Lee (SL) model, which provides a unified description of $\pi N \rightarrow \pi N$, $\gamma N \rightarrow \pi N$, and $N(e, e'\pi)N$ reactions up to the Δ-excitation region. The correlated-basis function (CBF) hole-SF [38,39] was used to account for the nuclear correlations in the initial target state. Predictions were also made for neutrino-induced inclusive ^{12}C(ν, μ) cross sections using the extended SL model [40], which also contains axial current contributions fit to $N(\nu, \mu\pi)N$ reactions data. On the other hand, two-nucleon $\gamma^* + NN \rightarrow NN$ mechanisms were not considered in that analysis.

In this work, we have implemented into the EFS the electroweak pion production amplitudes generated from the dynamical coupled-channel model [41–43] developed by the Argonne National Laboratory–Osaka University (ANL-Osaka) collaboration. The ANL-Osaka model is an extension of the SL model to include all important meson-baryon channels and all nucleon resonances up to invariant mass $W = 2$ GeV. The parameters of the ANL-Osaka model are determined [41,43] by fitting about 26 000 data points of the πN, $\gamma N \rightarrow \pi N$, ηN, $K\Lambda$, $K\Sigma$ data from the channel thresholds to $W \leqslant 2.1$ GeV. It had also been extended [42] to describe the data of neutrino-induced $N(\nu, \mu \pi)N$ transitions. The resulting model contains about 20 nucleon resonances, which include all of the four-star resonances listed by the Particle Data Group [44]. Clearly the use of the ANL-Osaka model makes this work significantly different from the above-mentioned references. It has to be noted that a more recent work [45] which utilized the Paschos-Lalakuklich amplitudes [46–48] only includes $P_{33}(1232)$, $D_{13}(1520)$, $P_{11}(1440)$, and $S_{11}(1535)$ resonances.

We have also significantly improved upon the treatment of medium effects in the Δ-component of the two-body current, whose importance was established in the investigation of pion-nucleus reactions, as reviewed in Ref. [31]. On the same line as Ref. [30], we introduce in the Δ propagator of the two-body current a Δ-nucleus potential. To account for the momentum-dependence of the medium effects, the latter is generated [49,50] from a Brueckner-Hartree-Fock calculation based on a coupled-channel $NN \oplus N\Delta \oplus \pi NN$ model [51–54].

To test the reliability of our approach, we first calculate the electron-^{12}C inclusive cross sections for a variety of kinematical setups, assessing the relative importance of the different reaction mechanisms. We also present results for neutrino and antineutrino-^{12}C scattering, induced by both neutral- and charged-current transitions. We refrain from presenting flux-folded calculations, since the latter require a

more refined treatment of final-state interactions (FSI), for both two-nucleon knockout and pion-production processes. In particular, as far as the pion-production region is concerned, the processes in which the pion produced in the interaction vertex is absorbed in the nuclear medium should be accounted for before meaningful comparison with data are made.

In Sec. III we report the expressions for the lepton-nucleus inclusive cross sections in terms of the relevant response functions. One- and two-body current reaction mechanisms are reviewed in Secs. III A and III B, while Sec. III C is devoted to pion-production processes. In Sec. IV we present our results on leptons scattering off ^{12}C and in Sec. V we state our conclusions.

II. FORMULATION OF ELECTROWEAK LEPTON-NUCLEUS INCLUSIVE CROSS SECTIONS

Let us consider a charge-changing process in which a neutrino (ν_ℓ) or an antineutrino ($\bar{\nu}_\ell$) with initial momentum $k^\mu = (E, \mathbf{k})$ scatters off a nuclear target, the final hadronic state being undetected. Denoting by $k'^\mu = (E', \mathbf{k}')$ the momentum of the outgoing lepton, the double-differential cross section in the Born approximation can be written as [55,56]

$$\left(\frac{d\sigma}{dE'd\Omega'}\right)_{\nu_\ell/\bar{\nu}_\ell} = \frac{G_F^2 \cos^2 \theta_c}{4\pi^2} k' E' L_{\mu\nu} W^{\mu\nu}. \quad (1)$$

We take $\cos \theta_c = 0.97425$ [44] and for the Fermi coupling constant we adopt the value $G_F = 1.1803 \times 10^{-5}$ GeV^{-2}, as from the analysis of $0^+ \rightarrow 0^+$ nuclear β decays of Ref. [57], which accounts for the bulk of the inner radiative corrections [58].

The leptonic tensor is fully determined by the kinematics of the leptons in the initial and final states

$$L_{\mu\nu} = \frac{1}{EE'}(k_\mu k'_\nu + k'_\mu k_\nu - g_{\mu\nu} k \cdot k' \pm i\epsilon_{\mu\rho\nu\sigma} k^\rho k'^\sigma), \quad (2)$$

where the $+$ $(-)$ sign is for ν_ℓ $(\bar{\nu}_\ell)$ initiated reactions. The hadronic tensor, containing all information on strong-interaction dynamics of the target nucleus, is defined in terms of the transition between the initial and final nuclear states $|\Psi_0\rangle$ and $|\Psi_f\rangle$ with energies E_0 and E_f. For spin-zero nuclei it can be cast in the form

$$W^{\mu\nu} = \sum_f \langle\Psi_0|j_{CC}^{\mu\dagger}|\Psi_f\rangle\langle\Psi_f|j_{CC}^{\nu}|\Psi_0\rangle\delta(E_0 + \omega - E_f), \quad (3)$$

where the charged-current operator is the sum of vector and axial components $j_V^\mu + j_A^\mu$.

Taking the three-momentum transfer along the z axis and the total three-momentum in the x-z plane

$$\begin{aligned} q &= k - k' = (\omega, \mathbf{q}), \quad \mathbf{q} = (0, 0, q_z), \\ Q &= k + k' = (\Omega, \mathbf{Q}), \quad \mathbf{Q} = (Q_x, 0, Q_z), \end{aligned} \quad (4)$$

performing the Lorentz contraction in Eq. (1) yields

$$\begin{aligned} \left(\frac{d\sigma}{dE'd\Omega'}\right)_{\nu/\bar{\nu}} &= \frac{G_F^2 \cos^2 \theta_c}{4\pi^2} \frac{k'}{2E_\nu}[\hat{L}_{CC}R_{CC} + 2\hat{L}_{CL}R_{CL} \\ &\quad + \hat{L}_{LL}R_{LL} + \hat{L}_T R_T \pm 2\hat{L}_{T'}R_{T'}], \end{aligned} \quad (5)$$

where the kinematical factors are given by

$$\hat{L}_{CC} = \Omega^2 - q_z^2 - m_\ell^2,$$
$$\hat{L}_{CL} = (-\Omega Q_z + \omega q_z),$$
$$\hat{L}_{LL} = Q_z^2 - \omega^2 + m_\ell^2, \qquad (6)$$
$$\hat{L}_T = \frac{Q_x^2}{2} - q^2 + m_\ell^2,$$
$$\hat{L}_{T'} = \Omega q_z - \omega Q_z,$$

and $m_\ell^2 = k'^2$ is the mass of the outgoing lepton. The five electroweak response functions are expressed in terms of the hadron tensor components as

$$R_{CC} = W^{00},$$
$$R_{CL} = -\frac{1}{2}(W^{03} + W^{30}),$$
$$R_{LL} = W^{33},$$
$$R_T = W^{11} + W^{22}, \qquad (7)$$
$$R_{T'} = -\frac{i}{2}(W^{12} - W^{21}).$$

Note that the inclusive cross section of an electron scattering off a nucleus in the one-photon exchange approximation can be written in a similar fashion as in Eq. (1), provided that $G^2/4\pi^2$ is replaced by $2\alpha^2/q^4$, where $\alpha \simeq 1/137$ is the fine structure constant, and the contribution proportional to the Levi-Civita tensor is dropped from the leptonic tensor of Eq. (2). Hence, the double-differential cross section for this process reads

$$\left(\frac{d\sigma}{dE'd\Omega'}\right)_e = \left(\frac{d\sigma}{d\Omega'}\right)_M [\hat{A}_{CC} R_{CC} + \hat{A}_T R_T], \qquad (8)$$

where

$$\hat{A}_{CC} = \left(\frac{q^2}{q_z^2}\right)^2, \quad \hat{A}_T = -\frac{1}{2}\frac{q^2}{q_z^2} + \tan^2\frac{\theta}{2}, \qquad (9)$$

θ being the lepton scattering angle and

$$\left(\frac{d\sigma}{d\Omega'}\right)_M = \left[\frac{\alpha\cos(\theta/2)}{2E'\sin^2(\theta/2)}\right]^2 \qquad (10)$$

is the Mott cross section. The electromagnetic responses of Eq. (8) are written in terms of the hadron tensor components as in Eq. (7), provided that j_{CC}^μ is replaced by the electromagnetic current j_{EM}^μ, which is related to j_{VC}^μ through the conserved vector current (CVC) hypothesis. Because of their striking similarities and common ingredients, it is evident that a prerequisite for any reliable model of neutrino-nucleus scattering is its capability of accurately describing the large body of measured electron-scattering cross sections [59].

III. EXTENDED IMPULSE APPROXIMATION

The initial state of the target nucleus appearing in Eq. (3) does not depend on momentum transfer and can be safely treated within nuclear many-body theory (NMBT) regardless of the kinematics of the scattering. Within this scheme, the

nucleus is viewed as a collection of A pointlike protons and neutrons, whose dynamics are described by the nonrelativistic Hamiltonian

$$H = \sum_i \frac{\mathbf{p}_i^2}{2m_N} + \sum_{j>i} v_{ij} + \sum_{k>j>i} V_{ijk}. \qquad (11)$$

In the above equation, $\mathbf{p}_i$ is the momentum of the ith nucleon of mass m_N, while the potentials v_{ij} and V_{ijk} model the nucleon-nucleon (NN) and three-nucleon ($3N$) interactions, respectively. Up to moderate values of the momentum transfer, typically $|\mathbf{q}| \lesssim 500\,\text{MeV}$, NMBT can be applied to compute the response functions of $A \leqslant 12$ nuclei using initial- and final-state nuclear wave functions derived from the Hamiltonian of Eq. (11). In particular, virtually exact Green's function Monte Carlo (GFMC) calculations have shown that the strength and energy-dependence of two-nucleon processes induced by correlation effects and interaction currents are crucial in providing the most accurate description of electron- and neutrino-nucleus scattering in the quasielastic regime [17,60].

At large values of energy and momentum transfer, a calculation of the hadron tensor solely based on NMBT is no longer reliable. In this regime, the final state includes at least one particle carrying a large momentum $\sim\mathbf{q}$, and fully relativistic expressions of the transition currents need to be retained. The impulse approximation (IA) scheme allows one to circumvent the difficulties associated with the relativistic treatment of $|\Psi_f\rangle$ and of the current operator, while at the same time preserving essential features (such as correlations) inherent to a realistic description of nuclear dynamics.

A. One-body current processes

The IA scheme is based on the tenet that for $|\mathbf{q}| \gg 1/d$, d being the average nucleon-nucleon separation distance in the target, the struck nucleon is largely decoupled from the spectator ($A - 1$) particles [1,24]. Within the original implementation of the IA, the nuclear current operator reduces to a sum of one-body terms

$$j^\mu = \sum_i j_i^\mu \qquad (12)$$

and the nuclear final state factorizes as

$$|\psi_f^A\rangle \to |p\rangle \otimes |\psi_f^{A-1}\rangle. \qquad (13)$$

In the above equation $|p\rangle$ denotes the final-state nucleon with momentum $\mathbf{p}$ and energy $e(\mathbf{p}) = \sqrt{\mathbf{p}^2 + m_N^2}$, while $|\psi_f^{A-1}\rangle$ describes the ($A - 1$)-body spectator system. Its energy and recoiling momentum are fixed by energy and momentum conservation

$$E_f^{A-1} = \omega + E_0 - e(\mathbf{p}), \quad \mathbf{P}_f^{A-1} = \mathbf{q} - \mathbf{p}. \qquad (14)$$

Employing the factorized expression of the nuclear final state in Eq. (3) and inserting a single-nucleon completeness relation, the incoherent contribution to the one-body (1b) hadron tensor is given by

$$W_{1b}^{\mu\nu}(\mathbf{q}, \omega) = \int \frac{d^3k}{(2\pi)^3} dE P_h(\mathbf{k}, E) \frac{m_N^2}{e(\mathbf{k})e(\mathbf{k}+\mathbf{q})}$$

$$\times \sum_i \langle k | j_i^{\mu\dagger} | k+q \rangle \langle k+q | j_i^\nu | k \rangle$$

$$\times \delta(\omega - E + m_N - e(\mathbf{k}+\mathbf{q})), \qquad (15)$$

where m_N is the rest mass contribution to the energy of the initial nucleon. The energy conserving δ function can be rewritten as $\delta(\tilde{\omega} + e(\mathbf{k}) - e(\mathbf{k}+\mathbf{q}))$ with $\tilde{\omega} = \omega - E + m_N - e(\mathbf{k})$. Hence, the scattering on a bound nucleon carrying momentum $\mathbf{k}$ is given in terms of the tensor describing the scattering off a free nucleon where the four-momentum transfer is replaced by $q = (\omega, \mathbf{q}) \to \tilde{q} = (\tilde{\omega}, \mathbf{q})$. The factors $m_N/e(\mathbf{k})$ and $m_N/e(\mathbf{k}+\mathbf{q})$ are included to account for the implicit covariant normalization of the four-spinors of the initial and final nucleons in the matrix elements of the relativistic current. The hole spectral function

$$P_h(\mathbf{k}, E) = \sum_f \left| \langle \psi_0^A | [|k\rangle \otimes |\psi_f^{A-1}\rangle] \rangle \right|^2 \delta(E + E_f^{A-1} - E_0^A) \qquad (16)$$

provides the probability distribution of removing a nucleon with momentum $\mathbf{k}$ from the target nucleus, leaving the residual $(A-1)$-nucleon system with an excitation energy E. Note that in Eq. (15) we neglected Coulomb interactions and the other (small) isospin-breaking terms and made the assumption, largely justified in the case of symmetric isospin zero $(T=0)$ nuclei, that the proton and neutron spectral functions are identical.

Within the correlated-basis function theory (CBF), the hole SF of finite nuclei is expressed as a sum of two contributions [39], displaying distinctly different energy and momentum dependences

$$P_h(\mathbf{k}, E) = P_h^{1h}(\mathbf{k}, E) + P_h^{corr}(\mathbf{k}, E). \qquad (17)$$

The one-hole term, corresponding to bound $A-1$ states, is obtained from a modified mean-field scheme

$$P_h^{1h}(\mathbf{k}, E) = \sum_{\alpha \in \{F\}} Z_\alpha |\phi_\alpha(\mathbf{k})|^2 F_\alpha(E - e_\alpha), \qquad (18)$$

where the sum runs over all occupied single-particle nuclear states, labeled by the index α, and $\phi_\alpha(\mathbf{k})$ is the Fourier transform of the shell-model orbital with energy e_α. The *spectroscopic* factor $Z_\alpha < 1$ and the function $F_\alpha(E - e_\alpha)$, describing the energy width of the state α, account for the effects of residual interactions that are not included in the mean-field picture. In the absence of the latter, $Z_\alpha \to 1$ and $F_\alpha(E - e_\alpha) \to \delta_\alpha(E - e_\alpha)$. The spectroscopic factors and the widths of the s and p states of ^{12}C used in this work are from the analysis of $(e, e'p)$ data carried out in Refs. [61–63].

The correlated part of the SF for finite nuclei $P_h^{corr}(\mathbf{k}, E)$ corresponds to unbound $|\psi_f^{A-1}\rangle$ states in Eq. (16), in which at least one of the spectators is in the continuum. It is obtained through the local density approximation (LDA) procedure

$$P_h^{corr}(\mathbf{k}, E) = \int d^3R\, \rho_A(\mathbf{R}) P_{h,NM}^{corr}(\mathbf{k}, E; \rho_A(\mathbf{R})). \qquad (19)$$

In the above equation, $\rho_A(\mathbf{R})$ is the nuclear density distribution of the nucleus and $P_{h,NM}^{corr}(\mathbf{k}, E; \rho)$ is the correlation component of the SF of isospin-symmetric nuclear matter

at density ρ, which vanishes if nuclear correlations are not accounted for. The use of the LDA to account for $P_h^{corr}(\mathbf{k}, E)$ is justified by the fact that to a remarkably large extent short-range nuclear dynamics is unaffected by surface and shell effects. The energy-dependence exhibited by $P_h^{corr}(\mathbf{k}, E)$, showing a widespread background extending up to large values of both k and E, is completely different from that of $P_h^{1h}(\mathbf{k}, E)$. For $k > p_F$, $P_h^{corr}(\mathbf{k}, E)$ coincides with $P_h(\mathbf{k}, E)$ and its integral over the energy gives the so-called continuous part of the momentum distribution.

The distinct momentum dependences of the one-hole and the correlated part of the hole SF can be appreciated by comparing the momentum distributions corresponding to $P_h(\mathbf{k}, E)$ and $P_h^{1h}(\mathbf{k}, E)$, displayed in Fig. 1. In this figure we also show the free Fermi gas momentum distribution for $k_F = 225$ MeV and the one computed within variational Monte Carlo (VMC) using a Hamiltonian comprised of the Argonne v_{18} [64] and the Urbana X [15] potentials. It is clear that the correlation component enhances the high-momentum tail of the hole SF bringing the corresponding momentum distribution in good agreement with the VMC results [65]. On the other hand, the differences with the free Fermi gas approximation are striking: $n^{FG}(\mathbf{k})$ is flat for $|\mathbf{k}| < k_F$ and vanishes for $|\mathbf{k}| > k_F$.

In the kinematical region in which the interactions between the struck particle and the spectator system cannot be neglected, the IA results have to be modified to include the effect of FSI. Following Ref. [66], we consider the real part of the optical potential U derived from the Dirac phenomenological fit of Ref. [67] to describe the propagation of the knocked-out particle in the mean-field generated by the spectator system. This potential, given as a function of the kinetic energy of the nucleon $t_{kin}(\mathbf{p}) = \sqrt{\mathbf{p}^2 + m^2} - m$, modifies the energy spectrum of the struck nucleon as

$$\tilde{e}(\mathbf{k}+\mathbf{q}) = e(\mathbf{k}+\mathbf{q}) + U(t_{kin}(\mathbf{k}+\mathbf{q})). \qquad (20)$$

The multiple scatterings that the struck particle undergoes during its propagation through the nuclear medium are taken into account through a convolution scheme. The IA responses
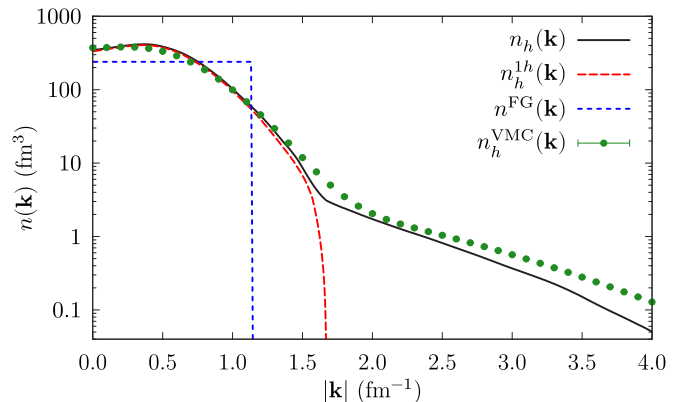

FIG. 1. Momentum distributions associated with the hole SF [$n_h(\mathbf{k})$], the mean-field component of the hole SF [$n_h^{1h}(\mathbf{k})$], the free Fermi gas at $k_F = 225$ MeV [$n^{FG}(\mathbf{k})$], and the VMC results of [65] [$n_h^{VMC}(\mathbf{k})$].

are folded with the function $f_{\mathbf{k}+\mathbf{q}}$, normalized as

$$\int_{-\infty}^{+\infty} d\omega f_{\mathbf{k}+\mathbf{q}}(\omega) = 1 . \qquad (21)$$

The one-body hadron tensor then reads

$$W_{1b}^{\mu\nu}(\mathbf{q}, \omega) = \int \frac{d^3k}{(2\pi)^3} dE P_h(\mathbf{k}, E) \int d\omega' f_{\mathbf{k}+\mathbf{q}}(\omega - \omega')$$

$$\times \frac{m_N^2}{e(\mathbf{k})e(\mathbf{k}+\mathbf{q})} \sum_i \langle k|j_i^{\mu\dagger}|k+q\rangle\langle k+q|j_i^\nu|k\rangle$$

$$\times \delta(\omega' + E - \tilde{e}(\mathbf{k}+\mathbf{q}))\theta(|\mathbf{k}+\mathbf{q}| - p_F). \qquad (22)$$

The folding function is computed within a generalization of the Glauber theory [68]

$$f_{\mathbf{p}}(\omega) = \delta(\omega)\sqrt{T_{\mathbf{p}}} + \int \frac{dt}{2\pi} e^{i\omega t}\left[\bar{U}_{\mathbf{p}}^{FSI}(t) - \sqrt{T_{\mathbf{p}}}\right]$$

$$= \delta(\omega)\sqrt{T_{\mathbf{p}}} + (1 - \sqrt{T_{\mathbf{p}}})F_{\mathbf{p}}(\omega). \qquad (23)$$

Full expressions for the nuclear transparency $T_{\mathbf{p}}$ and for the finite width function $F_{\mathbf{p}}(\omega)$ can be found in [24,69].

The one-body CC operator is the sum of a vector and axial component

$$j_{CC}^\mu = j_V^\mu + j_A^\mu,$$

$$j_V^\mu = \mathcal{F}_1\gamma^\mu + i\sigma^{\mu\nu}q_\nu\frac{\mathcal{F}_2}{2m_N}, \qquad (24)$$

$$j_A^\mu = -\gamma^\mu\gamma_5\mathcal{F}_A - q^\mu\gamma_5\frac{\mathcal{F}_p}{m_N},$$

where

$$\mathcal{F}_1 = F_1^V\tau_\pm.$$

$$\mathcal{F}_2 = F_2^V\tau_\pm, \qquad (25)$$

and $\tau_\pm = (\tau_x \pm i\tau_y)/2$ is the isospin raising/lowering operator. The Dirac and Pauli form factors defining $F_{1,2}^V = F_{1,2}^p - F_{1,2}^n$ are usually written in terms of the Sachs form factors as

$$F_1^{p,n} = \frac{G_E^{p,n} + \tau G_M^{p,n}}{1 + \tau},$$

$$F_2^{p,n} = \frac{G_M^{p,n} - G_E^{p,n}}{1 + \tau} \qquad (26)$$

with $\tau = -q^2/4m_N^2$. The axial term of the CC can be cast in the form

$$\mathcal{F}_A = F_A\tau_\pm,$$

$$\mathcal{F}_P = F_P\tau_\pm. \qquad (27)$$

We employ the standard dipole parametrization for the axial form factor

$$F_A = \frac{g_A}{\left(1 - q^2/m_A^2\right)^2}, \qquad (28)$$

where the nucleon axial-vector coupling constant is taken to be $g_A = 1.2694$ [44] and the axial mass $m_A = 1.049$ GeV. Uncertainties in the Q^2 dependence of the axial form factor impact neutrino-nucleus cross-section predictions. In this

regard, the dipole parametrization has been the subject of intense debate: dedicated lattice-QCD calculations of $G_A(Q^2)$ have been carried out [70] and an alternative "z-expansion" analysis [71] has been recently proposed.

Partially conserved axial current (PCAC) arguments connect the pseudoscalar form factor to the axial one

$$F_P = \frac{2m_N^2}{(m_\pi^2 - q^2)}F_A, \qquad (29)$$

m_π being the pion mass. While F_P can be safely neglected when considering ν_e, ν_μ-induced processes, its contribution cannot be ignored for a heavy τ lepton production and in the analysis of muon-capture processes [72,73].

The conserved-vector-current (CVC) hypothesis allows one to relate the vector component of the CC current to the EM: $j_{EM}^\mu = j_V^\mu$, provided that

$$\mathcal{F}_1 = \tfrac{1}{2}\left[F_1^S + F_1^V\tau_z\right],$$

$$\mathcal{F}_2 = \tfrac{1}{2}\left[F_2^S + F_2^V\tau_z\right], \qquad (30)$$

where $F_{1,2}^S = F_{1,2}^p + F_{1,2}^n$ is the single-nucleon isoscalar form factor.

B. Inclusion of two-body currents

In the last few years, the IA scheme has been generalized to include meson-exchange currents, which naturally arise from the dynamics of the constituent nucleons. For instance, the gauge invariance of the theory imposes that the electromagnetic charge and current operators satisfy the continuity equation $\mathbf{q} \cdot \mathbf{j}_{EM} = [H, j_{EM}^0]$. Since the two- and three-nucleon potentials of Eq. (11) do not commute with the charge operator j^μ must comprise two- and three-nucleon contributions. Neglecting the latter, which have numerically proven to be very small in $A = 3$ observables [74], we can write the CC and EM currents as

$$j^\mu = \sum_i j_i^\mu + \sum_{i<j} j_{ij}^\mu. \qquad (31)$$

In Refs. [25–27] the factorization ansatz of Eq. (13) has been extended to treat the amplitudes involving two-nucleon currents consistently with the correlation component of the hole SF

$$\left|\psi_f^A\right\rangle \to |pp'\rangle_a \otimes |\psi_f^{A-2}\rangle. \qquad (32)$$

where $|p\,p'\rangle_a = |p\,p'\rangle - |p'\,p\rangle$. In infinite isospin-symmetric nuclear matter, the pure two-body current component of the hadron tensor turns out to be [25]

$$W_{2b}^{\mu\nu}(\mathbf{q}, \omega)$$

$$= \frac{V}{4} \int dE \frac{d^3k}{(2\pi)^3} \frac{d^3k'}{(2\pi)^3} \frac{d^3p}{(2\pi)^3} \frac{m_N^4}{e(\mathbf{k})e(\mathbf{k}')e(\mathbf{p})e(\mathbf{p}')}$$

$$\times P_h^{NM}(\mathbf{k}, \mathbf{k}', E) 2\sum_{ij} \langle k\,k'|j_{ij}^{\mu\dagger}|p\,p'\rangle_a\langle p\,p'|j_{ij}^\nu|k\,k'\rangle$$

$$\times \delta(\omega - E + 2m_N - e(\mathbf{p}) - e(\mathbf{p}')). \qquad (33)$$

In the above equation, the normalization volume for the nuclear wave functions $V = \rho/A$ with $\rho = 3\pi^2 k_F^3/2$ depends

on the Fermi momentum of the nucleus, which for ^{12}C we take to be $k_F = 225$ MeV. The factor 1/4 accounts for the sum over indistinguishable pairs of particles, while the factor 2 arises from the fact that, renaming the dummy indexes, the product of the two direct terms is equal to the one of the two exchange terms [75]. In principle, the calculation of $W_{2b}^{\mu\nu}(\mathbf{q}, \omega)$ requires the knowledge of the two-nucleon hole spectral function of infinite nuclear matter $P_h^{\mathrm{NM}}(\mathbf{k}, \mathbf{k}', E)$. Within the CBF theory, it has been shown that, in absence of long-range correlations, the two-body momentum distribution factorizes as

$$\int dE P_h^{\mathrm{NM}}(\mathbf{k}, \mathbf{k}', E) = n(\mathbf{k}, \mathbf{k}') = n(\mathbf{k})n(\mathbf{k}') + \mathcal{O}\left(\frac{1}{A}\right). \tag{34}$$

Hence, the two-body current component of the hadron tensor can be expressed as

$$\begin{aligned} W_{2b}^{\mu\nu}(\mathbf{q}, \omega) = \frac{V}{2} \int d\tilde{E} \frac{d^3k}{(2\pi)^3} d\tilde{E}' \frac{d^3k'}{(2\pi)^3} \frac{d^3p}{(2\pi)^3} \\ \times \frac{m_N^4}{e(\mathbf{k})e(\mathbf{k}')e(\mathbf{p})e(\mathbf{p}')} P_h^{\mathrm{NM}}(\mathbf{k}, \tilde{E}) P_h^{\mathrm{NM}}(\mathbf{k}', \tilde{E}') \\ \times \sum_{ij} \langle k\,k' | j_{ij}^{\mu\dagger} | p\,p' \rangle_a \langle p\,p' | j_{ij}^{\nu} | k\,k' \rangle \\ \times \delta(\omega - \tilde{E} - \tilde{E}' + 2m_N - e(\mathbf{p}) - e(\mathbf{p}')). \end{aligned} \tag{35}$$

In analogy with the one-body case, we can introduce $\tilde{\omega} = \omega - \tilde{E} - \tilde{E}' + 2m_N - e(\mathbf{k}) - e(\mathbf{k}')$. The resulting expression for the energy conserving δ function,

$$\delta(\tilde{\omega} + e(\mathbf{k}) + e(\mathbf{k}') - e(\mathbf{p}) - e(\mathbf{p}')), \tag{36}$$

is the same as the one corresponding to the scattering on two free nucleons, provided that $q = (\omega, \mathbf{q}) \to \tilde{q} = (\tilde{\omega}, \mathbf{q})$. In order to treat atomic nuclei, following Ref. [27], we replace the hole SF of infinite matter with the one of ^{12}C,

$$P_h^{\mathrm{NM}}(\mathbf{k}, E) \to \frac{k_F^3}{6\pi^2} P_h(\mathbf{k}, E), \tag{37}$$

where $P_h(\mathbf{k}, E)$ is computed as in Eq. (17).

It has been argued that the strong isospin dependence of the two-nucleon momentum distribution, supported by experimental data, persist for nuclei even larger than ^{12}C [76–79], hence questioning the regime of applicability of Eq. (34). A viable strategy to gauge the limitations of the factorization of the two-body momentum distribution consists in approximating the latter with the so-called two-body decay function [80]

$$P_h^{\mathrm{NM}}(\mathbf{k}, \mathbf{k}', E) \to n(\mathbf{k}, \mathbf{k}')\delta(E - \bar{E}_f^{A-2}), \tag{38}$$

$\bar{E}_f^{A-2}$ being the average energy of the $A-2$ spectator system, and use variational Monte Carlo results for $n(\mathbf{k}, \mathbf{k}')$. Explorative calculations in this directions are ongoing and will be the subject of a dedicated work. In this regard, it has to be noted that in this work the interference between one- and two-body currents is disregarded. While in the two-nucleon knockout final states this contribution is relatively small [25,26], CBF calculations in infinite nuclear matter suggest that nuclear tensor correlations strongly enhance the

interference terms for final states associated with single-nucleon knock out processes [81]. This is compatible with the Green's function Monte Carlo results for the electromagnetic [60] and neutral-current response functions [17], in which the interference between one- and two-body currents dominates the total two-body current contribution, significantly enhancing the quasielastic peak region.

Analogously to the one-body case, the two-body CC operator is the sum of a vector and axial component. We use the expressions derived in Ref. [82] by coupling the pion-production amplitudes of Ref. [83] to a second nucleonic line. They can be traced back to four distinct interaction mechanisms, namely the pion in flight, seagull, pion-pole, and Δ excitations

$$j_{\mathrm{CC}}^{\mu} = (j_{\mathrm{pif}}^{\mu})_{\mathrm{CC}} + (j_{\mathrm{sea}}^{\mu})_{\mathrm{CC}} + (j_{\mathrm{pole}}^{\mu})_{\mathrm{CC}} + (j_{\Delta}^{\mu})_{\mathrm{CC}}. \tag{39}$$

The corresponding EM currents are obtained from the vector components of the j_{CC}^{μ} using CVC hypothesis. Detailed expressions for the first four terms of Eq. (39) can be found in Refs. [27,82]. Here, we only focus on the diagrams reported in Fig. 2 (and the corresponding two in which particles 1 and 2 are interchanged), which are associated with two-body current terms involving a Δ resonance in the intermediate state. Because of the purely transverse nature of this current, the form of its vector component is not subject to current-conservation constraints and its expression is largely model dependent. We adopted the parametrization of Ref. [83]. With the momentum variables specified in Fig. 2, it is of the following form:

$$\begin{aligned} (j_{\Delta}^{\mu})_{\mathrm{CC}} = \frac{3}{2} \frac{f_{\pi NN} f^*}{m_\pi^2} \Bigg\{ \Pi(k_2)_{(2)} \Bigg[\left(-\frac{2}{3}\tau^{(2)} + \frac{I_V}{3} \right)_{\pm} \\ \times F_{\pi NN}(k_2) F_{\pi N\Delta}(k_2)(j_a^{\mu})_{(1)} - \left(\frac{2}{3}\tau^{(2)} + \frac{I_V}{3} \right)_{\pm} \\ \times F_{\pi NN}(k_2) F_{\pi N\Delta}(k_2)(j_b^{\mu})_{(1)} \Bigg] + (1 \leftrightarrow 2) \Bigg\}, \end{aligned} \tag{40}$$
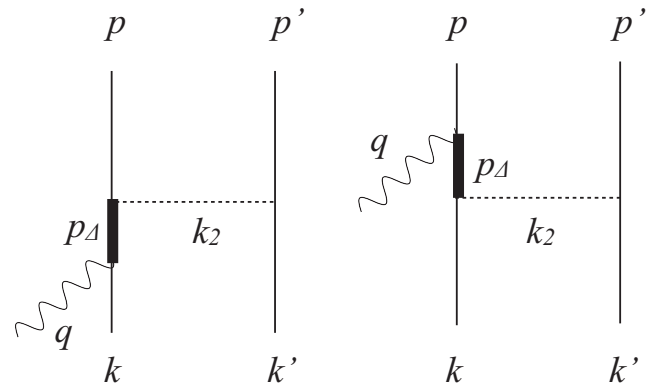

FIG. 2. Feynman diagrams describing two-body currents contributions associated to Δ excitation processes. Solid, thick, and dashed lines correspond to nucleons, deltas, and pions, respectively. The wavy line represents the vector boson.

where $k_2 = p' - k'$ is the momentum of the π exchanged in the two depicted diagrams, $f^* = 2.14$ and

$$\Pi(k) = \frac{\gamma_5 \slashed{k}}{k^2 - m_\pi^2}, \tag{41}$$

$$F_{\pi N \Delta}(k) = \frac{\Lambda_{\pi N \Delta}^2}{\Lambda_{\pi N \Delta}^2 - k^2}, \tag{42}$$

$$F_{\pi N N}(k) = \frac{\Lambda_\pi^2 - m_\pi^2}{\Lambda_\pi^2 - k^2} \tag{43}$$

with $\Lambda_{\pi N \Delta} = 1150 \, \text{MeV}$ and $\Lambda_\pi = 1300 \, \text{MeV}$. The isospin raising-lowering operator is given by

$$(I_V)_\pm = (\tau^{(1)} \times \tau^{(2)})_\pm , \tag{44}$$

where $\pm \to x \pm iy$.

In Eq. (40), j_a^μ and j_b^μ denote the $N \to \Delta$ transition vertices of the left and right diagrams, respectively. They are expressed as

$$j_a^\mu = (j_a^\mu)_V + (j_a^\mu)_A ,$$

$$(j_a^\mu)_V = \frac{C_3^V}{m_N} [k_2^\alpha G_{\alpha\beta}(p_\Delta)(g^{\beta\mu}\slashed{q} - q^\beta\gamma^\mu)]\gamma_5,$$

$$(j_a^\mu)_A = C_5^A [k_2^\alpha G_{\alpha\beta}(p_\Delta)g^{\beta\mu}], \tag{45}$$

where k is the momentum of the initial nucleon which absorbs the incoming momentum $\tilde{q}$ and $p_\Delta = \tilde{q} + k$, yielding $p_\Delta^0 = e(\mathbf{k}) + \tilde{\omega}$, and

$$j_b^\mu = (j_b^\mu)_V + (j_b^\mu)_A ,$$

$$(j_b^\mu)_V = \frac{C_3^V}{m_N} \gamma_5 [(g^{\alpha\mu}\slashed{q} - q^\alpha\gamma^\mu) G_{\alpha\beta}(p_\Delta)k_2^\beta],$$

$$(j_b^\mu)_A = C_5^A [g^{\alpha\mu} G_{\alpha\beta}(p_\Delta)k_2^\beta], \tag{46}$$

where p is the outgoing nucleon four-momentum and $p_\Delta = p - \tilde{q}$. In the above equations all nucleons are on the mass shell with the time component $p^0 = \sqrt{m_N^2 + \vec{p}^2}$.

The Rarita-Schwinger propagator

$$G^{\alpha\beta}(p_\Delta) = \frac{P^{\alpha\beta}(p_\Delta)}{p_\Delta^2 - M_\Delta^2} \tag{47}$$

is proportional to the spin 3/2 projection operator

$$P^{\alpha\beta}(p_\Delta) = (\slashed{p}_\Delta + M_\Delta) \left[g^{\alpha\beta} - \frac{1}{3}\gamma^\alpha\gamma^\beta - \frac{2}{3}\frac{p_\Delta^\alpha p_\Delta^\beta}{M_\Delta^2} \right.$$

$$\left. + \frac{1}{3}\frac{p_\Delta^\alpha\gamma^\beta - p_\Delta^\beta\gamma^\alpha}{M_\Delta} \right]. \tag{48}$$

The possible decay of the Δ into a physical πN state is accounted for by replacing the real resonance mass $M_\Delta = 1232 \, \text{MeV}$ entering the free propagator of Eq. (47) by $M_\Delta - i\Gamma(p_\Delta)/2$ [84,85]. The energy-dependent decay width $\Gamma(p_\Delta)/2$, effectively describing the allowed phase space for the pion produced in the decay, is given by

$$\Gamma(p_\Delta) = -2\text{Im}[\Sigma_{\pi N}(p_\Delta)]$$

$$= \frac{(4f_{\pi N \Delta})^2}{12\pi m_\pi^2} \frac{|\mathbf{k}|^3}{\sqrt{s}} (m_N + E_k) R(\mathbf{r}^2), \tag{49}$$

where $\Sigma_{\pi N}(p_\Delta)$ is the Δ self-energy in vacuum. In the above equation, $(4f_{\pi N \Delta})^2/(4\pi) = 0.38$, $s = p_\Delta^2$ is the invariant mass, $\mathbf{k}$ is the decay three-momentum in the πN center of mass frame, such that

$$|\mathbf{k}|^2 = \frac{1}{4s}[s - (m_N + m_\pi)^2][s - (m_N - m_\pi)^2], \tag{50}$$

and $E_k = \sqrt{m_N^2 + \mathbf{k}^2}$ is the associated energy. The additional factor

$$R(\mathbf{r}^2) = \left(\frac{\Lambda_R^2}{\Lambda_R^2 - \mathbf{r}^2} \right) \tag{51}$$

depending on the πN three-momentum $\mathbf{r}$ with $\mathbf{r}^2 = (E_k - \sqrt{m_\pi^2 + \mathbf{k}^2})^2 - 4\mathbf{k}^2$ and $\Lambda_R^2 = 0.95 \, m_N^2$, is introduced to improve the description of the experimental phase-shift δ_{33} [84].

We now depart from the approach of Refs. [27,82,85,86] to consider medium effects on the Δ propagators depicted in the diagrams of Fig. 2. From the extensive study of pion-nucleus reactions, it has been well established that the Δ width can be modified by Pauli blocking of the $\Delta \to \pi N$ decay in medium and Δ can be annihilated by the nucleons in nuclei. A rigorous account for these many-body effects can only be achieved within the elaborated Δ-hole model [32–34] of pion-nucleus reactions and is beyond the scope of this work. As a first exploratory step, we will neglect the Pauli blocking effect and follow Refs. [31,49,50] to account for the annihilation of the Δ via $\Delta N \to NN$ interactions by introducing a shift of the Δ self-energy $\Sigma_{\pi N}(p_\Delta)$ in free space

$$\Sigma_{\pi N}(p_\Delta) \to \Sigma_{\pi N}(p_\Delta) + U_\Delta(\mathbf{p}_\Delta, \rho), \tag{52}$$

where $\mathbf{p}_\Delta$ is the three-momentum of the Δ and ρ is the nuclear density. We generate $U_\Delta(\mathbf{p}_\Delta, \rho)$ from a Brueckner-Hartree-Fock calculation using a coupled-channel $NN \oplus N\Delta \oplus \pi NN$ model [51–54]. Its real and imaginary parts, displayed in Fig 3, exhibit a relatively strong momentum dependence. To get a qualitative estimate of the medium effect, we will modify the decay width of Eq. (49) by including the imaginary part of $U_\Delta(p_\Delta, \rho)$ as

$$\Gamma_\Delta(p_\Delta) \to \Gamma_\Delta(p_\Delta) - 2\text{Im}[U_\Delta(p_\Delta, \rho = \rho_0)], \tag{53}$$

where we fixed the density at the nuclear saturation value $\rho_0 = 0.16 \, \text{fm}^3$.
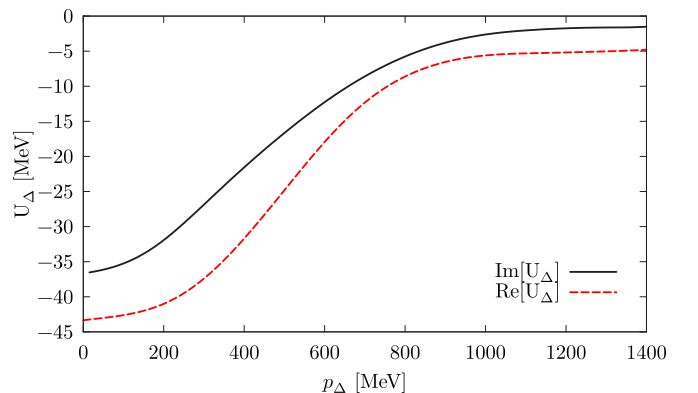

FIG. 3. Real and imaginary parts of the Δ potential in nuclear matter at saturation density $\rho = 0.16 \, \text{fm}^{-3}$.

C. Pion-production mechanisms

The primary goal of this work consists in further generalizing the factorization ansatz of Eq. (13) to accommodate productions of real pions in the final state. To this aim, the final state of the reaction can be cast into the form

$$\left| \psi_f^A \right\rangle \rightarrow \left| p_\pi p \right\rangle \otimes \left| \psi_f^{A-1} \right\rangle, \tag{54}$$

where p_π denotes both the four-momentum $(p_\pi^0, \mathbf{p}_\pi)$ and the isospin t_π of the emitted pion. Following the same steps that led to Eq. (15), the incoherent contribution to the one-body one-pion (1b1π) hadron tensor reads

$$W_{1b1\pi}^{\mu\nu}(\mathbf{q}, \omega)$$
$$= \int \frac{d^3k}{(2\pi)^3} dE P_h(\mathbf{k}, E) \frac{d^3 p_\pi}{(2\pi)^3} \frac{m_N^2}{e(\mathbf{k})e(\mathbf{k} + \mathbf{q} - \mathbf{p}_\pi)}$$
$$\times \sum_i \langle k| j_i^{\mu\dagger} |p_\pi p\rangle \langle p_\pi p| j_i^\nu |k\rangle \Big|_{\mathbf{p}=\mathbf{k}+\mathbf{q}-\mathbf{p}_\pi}$$
$$\times \delta(\omega - E + m_N - e(\mathbf{k} + \mathbf{q} - \mathbf{p}_\pi) - e_\pi(\mathbf{p}_\pi)), \tag{55}$$

where $e_\pi(\mathbf{p}_\pi) = \sqrt{\mathbf{p}_\pi^2 + m_\pi^2}$ is the energy of the outgoing pion. In this case the modified energy transfer is identical to the one of one-body current processes $\tilde{\omega} = \omega - E + m_N - e(\mathbf{k})$. Besides the additional integration over $\mathbf{p}_\pi$ the main difference between the above expression and Eq. (15) resides in the elementary amplitude. To describe the pion-production processes, we need matrix elements of the charged-current operator causing the transition from a bound nucleon $|k\rangle$ to a state with a pion and a nucleon $|p_\pi p\rangle$.

In this work, we employ the ANL-Osaka coupled-channel model [41–43] to generate the current matrix elements $\langle p_\pi p| j_i^\nu |k\rangle$ of Eq. (55). The ANL-Osaka model is defined by a Hamiltonian of the following form:

$$H_{AO} = H_0 + \sum_{c,c'} v_{c,c'} + \sum_{N^*} \sum_c [\Gamma_{N^*,c} + \Gamma_{N^*,c}^\dagger], \tag{56}$$

where H_0 is the free Hamiltonian, $\Gamma_{N^*,c}$ is a vertex defining the formation of a bare N^* state from a meson-baryon channel c. The channels included are $c, c' = \gamma N, \pi N, \eta N, K\Lambda, K\Sigma$, and $\pi\pi N$ with resonant $\pi\Delta$, ρN, and σN components. The energy independent meson-exchange potentials $v_{c,c'}$ are derived from phenomenological Lagrangians by using the unitary transformation method [36,92]. The parameters of the Hamiltonian H_{AO} have been determined in Refs. [41,43] by fitting about 26 000 data points of the $\pi N, \gamma N \rightarrow \pi N, \eta N, K\Lambda, K\Sigma$ data from the channel thresholds to $W \leqslant 2.1$ GeV. The resulting model generates about 20 nucleon resonances which include all of the four-stars resonances listed by the Particle Data Group [44]. Here we note that the Hamiltonian in Eq. (56) is consistent with the conventional nuclear Hamiltonian given in Eq. (11). Thus it can be used straightforwardly to generate the current matrix elements $\langle p_\pi p| j_i^\nu |k\rangle$ of Eq. (55).

The ANL-Osaka model was then extended to the electron- and neutrino-induced reactions [42,96]. The Q^2 dependence of the vector current has been determined by analyzing data for single-pion electroproduction and inclusive electron scattering. As an example, we show in Figs. 4 and 5 that the ANL-Osaka model can reasonably describe the data
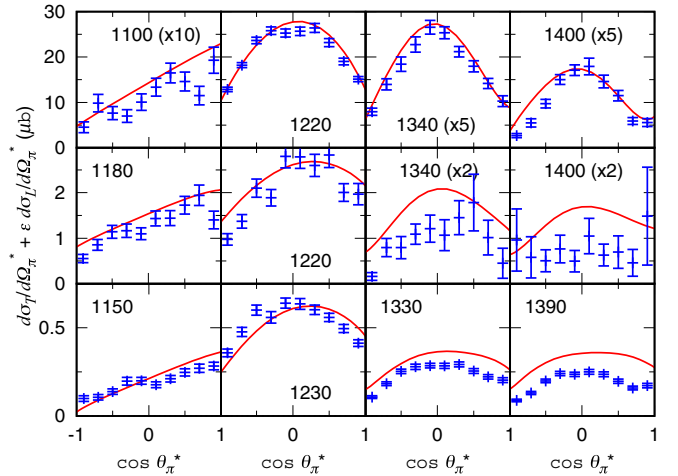

FIG. 4. Virtual-photon cross section $d\sigma_T/d\Omega^* + \epsilon d\sigma_L/d\Omega^*$ (μb/sr) calculated with the DCC model; $p(e, e'\pi^0)p$. The top, middle, and bottom rows present the cross sections at $Q^2 = 0.4$ $(\text{GeV}/c)^2$, $Q^2 = 1.76$ $(\text{GeV}/c)^2$, and $Q^2 = 2.95$ $(\text{GeV}/c)^2$, respectively. In each panel, the number indicates the invariant mass W (MeV), and the cross sections are scaled by the factor in the parenthesis. Experimental data are from Refs. [87,88].

of $p(e, e'\pi^0)p$ and $p(e, e'\pi^+)n$ reactions, respectively, for $Q^2 = 0.40$ $(\text{GeV}/c)^2$ (top), $Q^2 = 1.76$ $(\text{GeV}/c)^2$ (middle), $Q^2 = 2.95$ $(\text{GeV}/c)^2$ (bottom). On the other hand, the axial current associated with nucleon resonances cannot be determined very well because the neutrino-induced meson production data are scarce except in the $\Delta(1232)$ region. Thus we determined the axial couplings using the PCAC relation to the πN reaction amplitudes, and assumed the dipole Q^2 dependence with the cutoff of $\simeq 1$ GeV. For the bare axial nucleon-to-$\Delta(1232)$ coupling, we weaken the PCAC-based strength by 10% to better reproduce the neutrino data. In Figs. 6 and 7, we show that the neutrino data for the total cross sections and the Q^2 dependence of the single pion production can be described very well by the ANL-Osaka model.
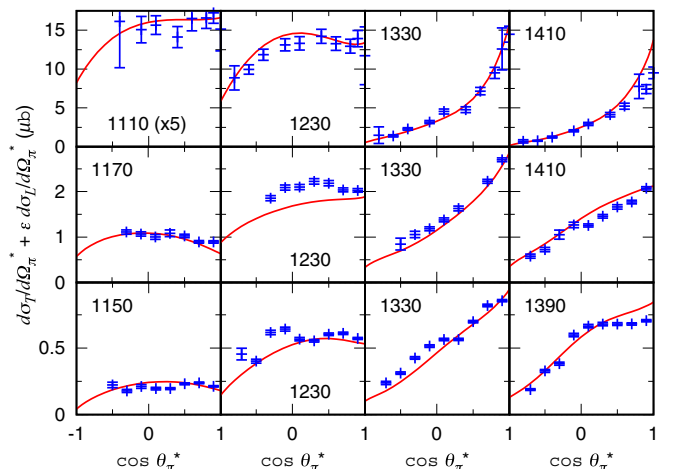

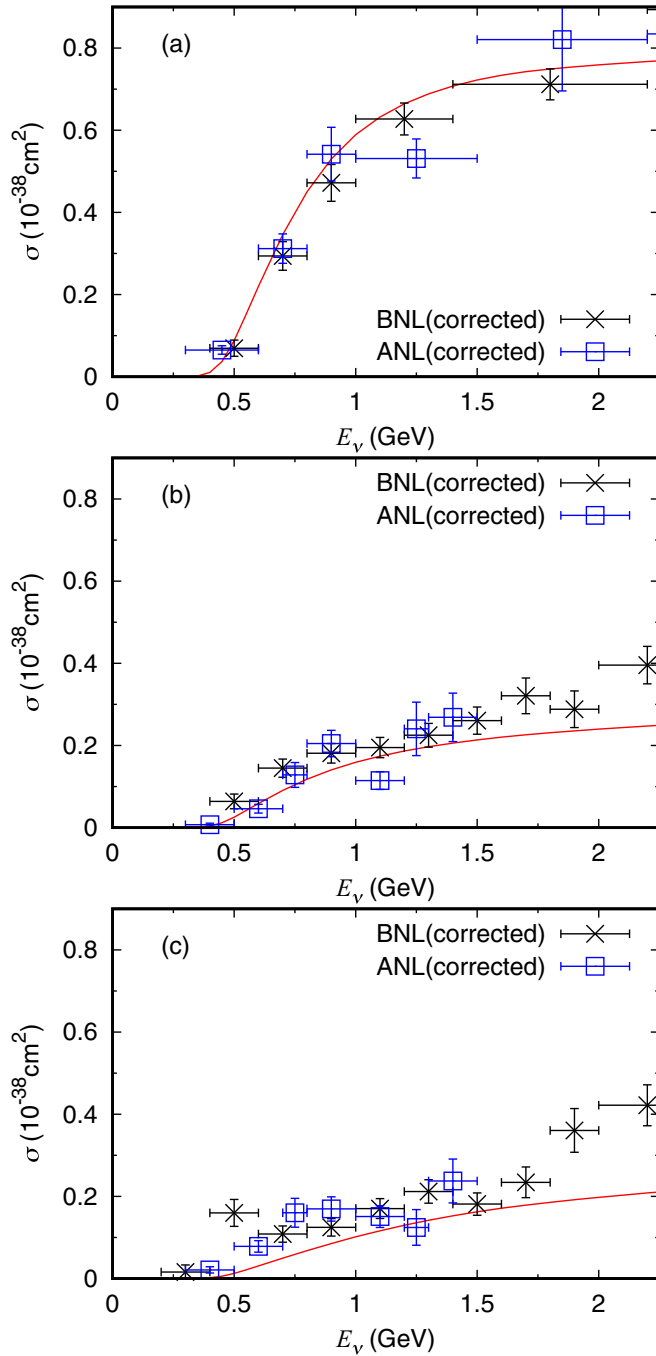FIG. 5. Same as Fig. 4 but for the $p(e, e'\pi^+)n$ reaction. Experimental data are from Refs. [89–91].

FIG. 6. Total cross sections of (a) $\nu_\mu p \to \mu^- \pi^+ p$; (b) $\nu_\mu n \to \mu^- \pi^0 p$; (c) $\nu_\mu n \to \mu^- \pi^+ n$. The solid red curves are from the DCC model. The data are from Ref. [93] where the ANL [94] and BNL [95] data have been corrected for the flux uncertainty.

FIG. 7. Flux-averaged (0.5 GeV $\leqslant E_\nu \leqslant$ 6 GeV) $d\sigma/dQ^2$ for $\nu_\mu p \to \mu^- \pi^+ p$. The solid red curves are from the DCC model. The data are from ANL [94] and BNL [95].

Here, we note that the PCAC relation with the πN amplitudes, and in particularly with their phases, is not taken into account in other pion production models, such as the Rein-Sehgal model [97]—commonly used in analyzing neutrino experiments—and the LPP model [46–48] recently employed to calculate inclusive processes [45] within the CBF hole SF formalism. This inconsistency leads to significant differences in the structure function F_2 at $Q^2 \sim 0$ [42].
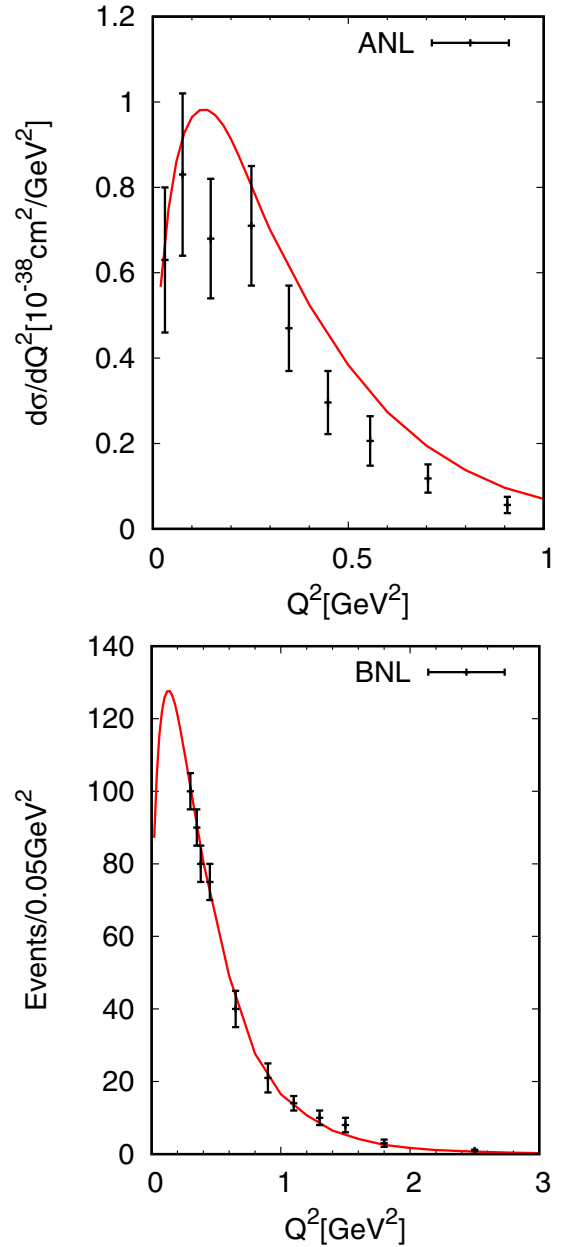
Prior to the present work, the ANL-Osaka DCC model has been applied to electroweak reactions on the simplest nucleus, the deuteron [98–101]. Predictions from the DCC-based model, which includes the impulse as well as NN and meson-nucleon rescattering mechanisms, agree reasonably well with the data on $\gamma d \to \pi NN$ [99,101] and $\gamma d \to \eta NN$ [98]. The model was also used to study final state interaction (FSI) effects on $\nu_\mu d \to \mu^- \pi NN$ [101], leading to the FSI corrections to the ANL [94] and BNL [95] data for $\nu_\mu N \to \mu^- \pi N$ which had been extracted from the deuteron target data without correcting for the significant FSI effects.

Analogously to these studies on the deuteron, in this work the DCC amplitudes in the laboratory frame are obtained by boosting the corresponding ones in the center-of-mass frame, where the DCC model was originally developed. Here, we briefly describe the procedures for calculating the current matrix elements $\langle p_\pi p | j_i^\nu(q) | k \rangle$ in Eq. (55) from those evaluated in the center of mass (c.m.) frame of πN. Including explicitly the nucleon spin quantum numbers m_s, we can write

$$
\langle p\, m_{s'}, p_\pi | j_i^\nu(q) | k\, m_s \rangle
$$
$$
= \sqrt{\frac{E_\pi(\mathbf{k}_c) E_N(-\mathbf{k}_c)}{E_\pi(\mathbf{p}_\pi) E_N(\mathbf{p})}} \sqrt{\frac{|\mathbf{q}_c| E_N(-\mathbf{q}_c)}{|\mathbf{q}| E_N(\mathbf{k})}} \sum_\mu \Lambda_\mu^\nu(p_t)
$$
$$
\times \left[\sum_{m'_{s_c}, m_{s_c}} R^*_{m'_{s_c}, m_{s'}}(p, p_t) R_{m_{s_c}, m_s}(k, p_t) \right.
$$
$$
\left. \times \langle \pi(\mathbf{k}_c), N(-\mathbf{k}_c\, m'_{s_c}) | j_i^\mu(q_c) | N(-\mathbf{q}_c\, m_{s_c}) \rangle \right], \quad (57)
$$

where the suffixes 'c' indicate quantities in the c.m. system of πN, $p_t = p + p_\pi = q + k$ is the total four-momentum of the πN system, defined by $\mathbf{p}_t = \mathbf{p} + \mathbf{p}_\pi = \mathbf{q} + \mathbf{k}$, and $p_t^0 = E_N(\mathbf{p}) + E_\pi(\mathbf{p}_\pi) = \omega + E_N(\mathbf{k})$. The c.m. matrix elements of the current operator, $\langle \pi(\mathbf{k}_c), N(-\mathbf{k}_c\, m'_{s_c}) | j_i^\mu(q_c) | N(-\mathbf{q}_c\, m_{s_c}) \rangle$, from the ANL-Osaka model are calculated following the procedure detailed in Appendix D of Ref. [41].

In Eq. (57), the quantity $\Lambda_\mu^\nu(p_t)$ boosts any momentum $a_c = (a_c^0, \boldsymbol{a}_c)$ in the c.m. of the considered πN system to the momentum $a_L = (a_L^0, \boldsymbol{a}_L)$ in the laboratory frame by the following Lorentz transformation:

$$
a_L^0 = \sum_\nu \Lambda_\nu^0(p_t) a_c^\nu = \frac{a_c^0 p_t^0 + \mathbf{p}_t \cdot \boldsymbol{a}_c}{m_t},
$$
$$
a_L^i = \sum_\nu \Lambda_\nu^i(p_t) a_c^\nu = a_c^i + p_t^i \left[\frac{\mathbf{p}_t \cdot \boldsymbol{a}_c}{m_t(m_t + p_t^0)} + \frac{a_c^0}{m_t} \right],
$$
$$
\quad (58)
$$

where the index $i = 1, 2, 3$ is a spatial component and $m_t \equiv \sqrt{p_t \cdot p_t}$.

The spin rotation matrix $R_{s_c, s}(p, p_t)$ in Eq. (57) is given [102–104] explicitly as

$$
R_{m_{s_c}, m_s}(p, p_t) = \langle m_{s_c} | B^{-1}(p_c/m_N) B^{-1}(p_t/m_t) B(p/m_N) | m_s \rangle,
$$
$$
\quad (59)
$$

where $|m_s\rangle$ is the nucleon spin state, p_c is obtained from the nucleon momentum p in the laboratory frame by the Lorentz transformation of Eq. (58), and

$$
B(p/m) = \frac{1}{\sqrt{2m(p^0 + m)}} ((p^0 + m)\mathbf{I} + \mathbf{p} \cdot \sigma),
$$
$$
B^{-1}(p/m) = \frac{1}{\sqrt{2m(p^0 + m)}} ((p^0 + m)\mathbf{I} - \mathbf{p} \cdot \sigma),
$$
$$
\quad (60)
$$

where σ is the Pauli operator and $\mathbf{I}$ is the unit matrix.

We note that because of the nuclear binding, the initial γN energy $q^0 + E_N(k)$ can be different from the final πN energy $E_N((p) + E_\pi(p_\pi)$. Following Refs. [99,101], we choose

$p_t = (E_N(p) + E_\pi(p_\pi), \mathbf{p} + \mathbf{k}_\pi)$ in evaluating Eqs. (57)–(60), and neglect the off-shell effects from the initial state in $\langle \pi(\mathbf{k}_c), N(-\mathbf{k}_c\, m'_{s_c}) | j_i^\mu(q_c) | N(-\mathbf{q}_c\, m_{s_c}) \rangle$.

IV. RESULTS

In the same manner as Ref. [27], the numerical integration of Eqs. (15), (35), (55) are carried out by means of a dedicated Metropolis Monte Carlo algorithm. Since the integrands extend up to large momentum and removal energy, when evaluating $W_{1b}^{\mu\nu}$ and $W_{1b1\pi}^{\mu\nu}$ it is convenient to employ a normalized hole-SF as the importance-sampling function. Analogously, the importance-sampling function of choice for $W_{2b}^{\mu\nu}$ is proportional to the product $P_h^{NM}(\mathbf{k}, \tilde{E}) P_h^{NM}(\mathbf{k}', \tilde{E}')$.

Figure 8 shows the MEC contribution to the double-differential electron-^{12}C cross section for $E_e = 730$ MeV and $\theta_e = 37°$. The solid (black) line corresponds to the full calculation in which the in-medium Δ-potential U_Δ has been included in the propagator, as explained in Sec. III B. On the other hand, the short-dashed (red) line is obtained disregarding this contribution. The comparison between the two curves clearly shows that accounting for the in-medium decay of the Δ leads to a visible quenching of the MEC contribution to the inclusive cross section. In Fig. 9 we show the effects of the in-medium potential of the Δ in the CC ν_μ-^{12}C scattering cross section for a beam energy $E_\nu = 1$ GeV and scattering angle $\theta_\mu = 30°$. In this particular kinematical setup, including U_Δ brings about a $\simeq 15\%$ depletion of the MEC strength. While the results shown in Figs. 8 and 9 exhibit similar trends, we observe that two-body currents play a more important role in neutrino reactions than in electron scattering. Most likely this is due to the difference between the V and $V - A$ vertex interactions with the Δ. The five electroweak nuclear responses displayed in Fig. 2 of Ref. [27] and Fig. 7 of Ref. [82] show that the vector contribution to the transverse response is twice as large as the electromagnetic term. This feature is ascribed to the traces of the two-body isospin operator entering the
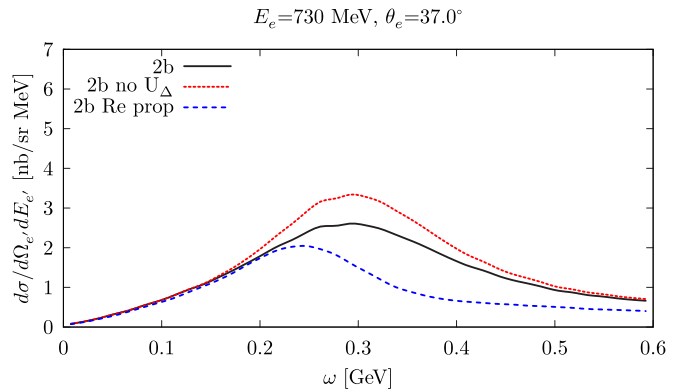
$$E_e = 730 \text{ MeV}, \ \theta_e = 37.0°$$

FIG. 8. Two-body current contribution to the double-differential electron-^{12}C cross section for $E_e = 730$ MeV and $\theta_e = 37°$. The solid (black) line corresponds to results in which the in-medium corrections to the Δ decay are included, while the short-dashed (red) line is obtained neglecting this contribution. The dashed (blue) line displays the two-body current contribution in which only the real part of the Δ propagator is retained.
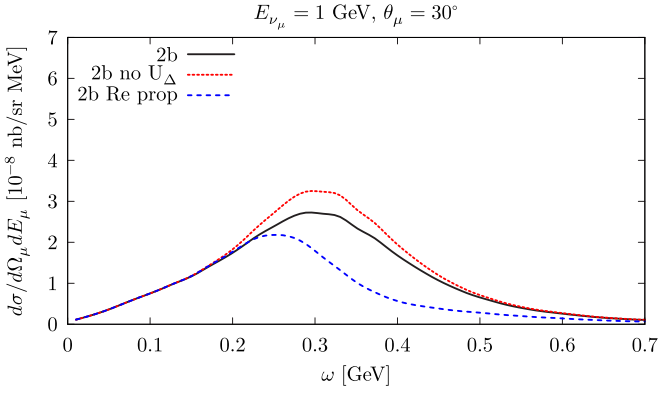
FIG. 9. Same as Fig. 8 but for CC ν_μ-^{12}C scattering at $E_{\nu_\mu} = 1$ GeV and $\theta_\mu = 30°$.

meson-exchange currents. Furthermore, the axial component of the currents leads to an enhancement of the longitudinal responses, as opposed to the electromagnetic case.

We also emphasize that the MEC contributions shown in Figs. 8 and 9 strongly depend on the parameters of Δ current illustrated in Fig. 2. In this work, we adopt the parameters used in the previous investigations [24,69]. This choice needs to be refined by developing a consistent approach to relate the Δ current operator to the ANL-Osaka model. Work in this direction is ongoing.

The way we include medium effects on the Δ propagation is significantly different from the prescription of keeping only the real part of Δ propagator [82,85,86], leading to the dashed (blue) lines of Figs. 8 and 9. Disregarding altogether the imaginary-part of the Δ propagator brings about a stronger reduction of the strength than including U_Δ. In addition, the position of the peak is shifted to lower energy transfers.

In Fig. 10 we compare the results obtained for the electron-^{12}C scattering double differential cross section for $E_e = 730$ MeV and $\theta_e = 37°$ employing different approximations to describe the nuclear target and the final state interactions. It has to be noted that, when computing the MEC contribution,
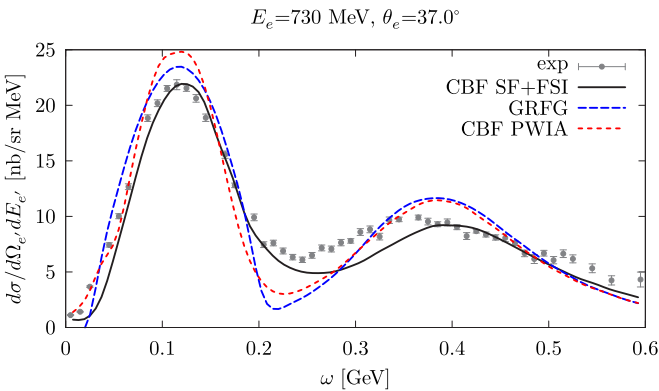

FIG. 10. Electron-^{12}C double-differential cross section. The dashed (blue) line has been obtained within the GRFG model. The short-dashed (red) and solid (black) curves have been obtained using the SF of Ref. [39] within the PWIA and IA with FSI corrections, respectively.

the two-body hole SF is approximated by the product of two one-body hole SF, as in Eq. (35). The cross sections with a real pion in the final state are computed convoluting the DCC elementary amplitudes with the one-nucleon SF, as discussed in Sec. III C, and a cut on invariant energies $W \leqslant 2.0$ GeV has been applied.

The dashed (blue) curve has been obtained using the global relativistic Fermi gas (GRFG) model, which only entails statistical correlations, to determine the hole SF

$$P_h^{\text{GRFG}}(\mathbf{k}, E) = \theta(k_F - |\mathbf{k}|)\delta\left(E + \frac{k^2}{2m}\right). \quad (61)$$

As for the Fermi momentum, we take $k_F = 225$ MeV and no binding energy is introduced. The short-dashed (red) line displays the plane wave impulse approximation (PWIA) result in which the excitation energies of the $(A-1)$-body spectator system are assumed to be constant, $E_f^{A-1} = \bar{E}^{A-1}$. Hence, the hole SF reduces to

$$P_h^{\text{PWIA}}(\mathbf{k}, E) = n_h(\mathbf{k})\delta\left(E + \bar{E}^{A-1} - E_0^A\right), \quad (62)$$

thereby losing information on the removal-energy distribution of the target. The momentum distribution employed in the PWIA calculations, represented by the black solid line of Fig. 1, is derived by integrating over the removal energy of the CBF hole SF of Ref. [39].

The solid (black) line in Fig. 10 is obtained using the full CBF hole SF to describe the quasielastic peak and the π-production regions. For this most sophisticated treatment of the target nucleus, we also show results in which the impulse approximation is corrected by including FSI. In single-nucleon knockout processes, this is achieved following Eqs. (21)–(23), i.e., employing the real part of an optical potential derived from the Dirac phenomenological fit of Ref. [67] and the folding function of Refs. [24,69]. The main two consequences of including FSI are a shift of the quasielastic peak and a redistribution of the strength towards lower values of ω. In two-nucleon emission processes, FSI are effectively accounted by including in their energy spectrum a momentum-independent binding of 60 MeV per particle. Treating FSI with the same level of sophistication as for the one-nucleon knockout requires the knowledge of the optical potential associated to the removal of two-nucleons from ^{12}C and the corresponding folding functions. In addition, single-charge exchange processes [105] and interactions taking place within the pair of struck nucleons should also be properly modeled. FSI between the π-nucleon state and the $A-1$ spectator system are not addressed in this article. For exclusive single pion production processes from neutrino-^{12}C scattering in the $\Delta(1232)$ region, it has been shown that pion absorptions and redistribution of the pion momentum spectrum are important FSI effects [106,107]. However, by definition, the (semi)classical treatments of the FSI therein employed do not modify the inclusive observables analyzed in the present work. A more systematic treatment of FSI in processes with both two outgoing nucleons and a pion and a nucleon in the final state is currently being investigated and will be the subject of a forthcoming work.

By comparing the solid with the dashed and short-dashed lines it clearly emerges that an accurate treatment of nuclear
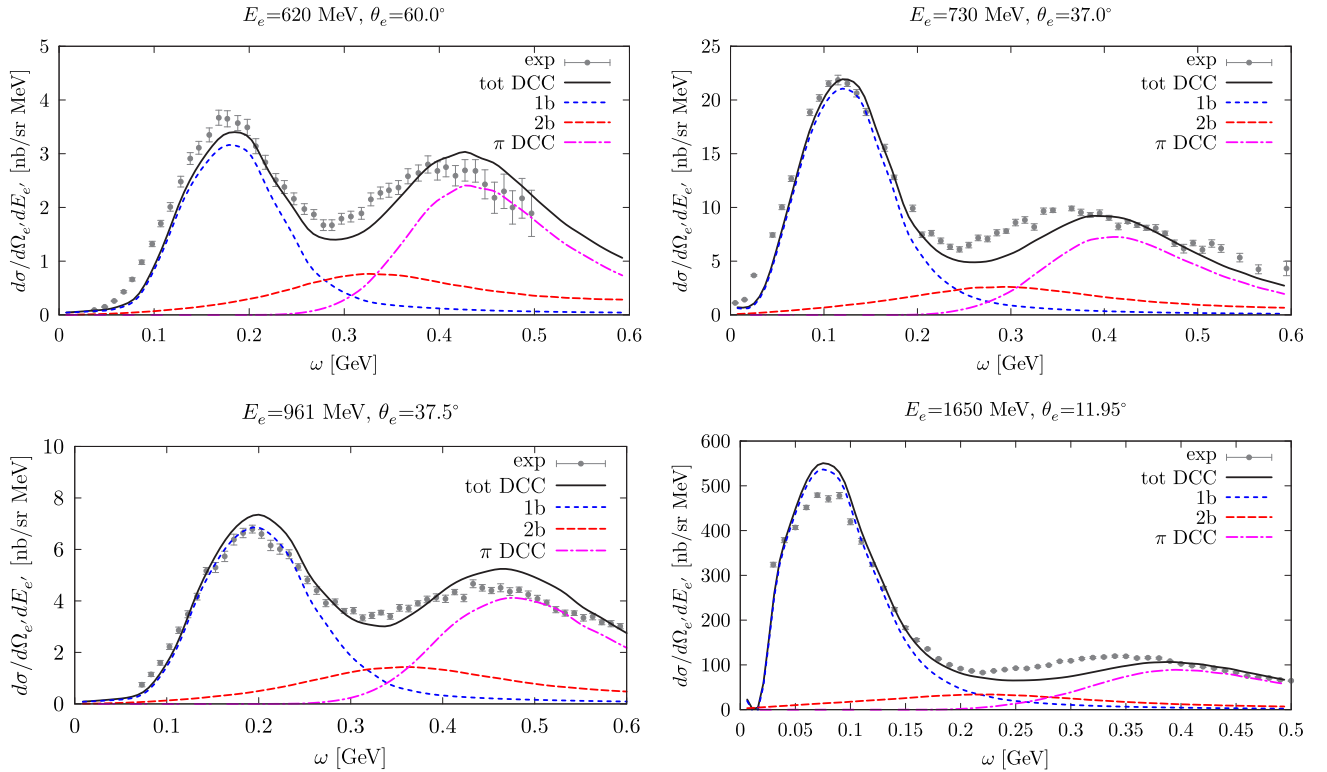
FIG. 11. Electron-^{12}C inclusive cross sections for different combinations of E_e and θ_e. The short-dashed (blue) line and dashed (red) line correspond to one- and two-body current contributions, respectively. The dash-dotted (magenta) lines represent π production contributions. The solid (black) line is the total results obtained summing the three different terms.

dynamics in the initial state and the inclusion of FSI considerably improve the agreement with experimental data in the whole energy-transfer region. For this particular kinematical setup, neglecting the correlations between the removal energy and momentum, as in the PWIA, leads to an overshooting of the quasielastic peak, even compared to the crudest GRFG model. This is consistent with Ref. [108] where the use of a realistic hole SF was found to produce noticeably different scaling features of the nucleon-density response from those obtained within the simple PWIA.

Figure 11 displays the double-differential electron-^{12}C cross sections in four kinematical setups, corresponding to: $E_e = 620$ MeV, $\theta_e = 60°$ (upper-left panel), $E_e = 730$ MeV, $\theta_e = 37°$ (upper-right panel), $E_e = 961$ MeV, $\theta_e = 37.5°$ (lower-left panel), and $E_e = 1650$ MeV, $\theta_e = 11.95°$ (lower-right panel). The total cross section, represented by the solid (black) line, is obtained as in Fig. 10 using the CBF hole-SF of Ref. [39] and including FSI as discussed above. The breakdown of the contributions associated with the different reactions mechanisms is also shown. The dashed (blue) line is the quasielastic peak obtained including the one-body current only, while the short-dashed (red) line corresponds to two-nucleon knockout final states induced by MEC reaction mechanisms. The cross section associated with the emission of a real pion and a nucleon is represented by the dot-dashed (magenta) line.

In all kinematical setups, MEC enhance the cross section primarily in the dip region, between the quasielastic and the

Δ peaks. Their strength exhibits a strong dependence on the electron scattering angle; it increases relatively to the one of one-body processes for larger values of the scattering angle. This is consistent with the findings of Ref. [27] and can be traced back to the fact that two-body currents are most effective in transverse responses. Note that, as discussed in Sec. III B, the interference between one- and two-body currents is not included in our calculations. Although it was argued in Ref. [25] that this leads to a small enhancement in the dip region within the factorization scheme, GFMC calculations have demonstrated that the interference contribution significantly increases the transverse electroweak responses [17,60].

There is an overall good agreement between theoretical results and experimental data in all the kinematical setups we considered. In particular, the inclusion of realistic pion production mechanism turns out to be essential to reproduce the data in the Δ-production region. Comparing our findings with those of Ref. [26], it appears that the DCC model largely overcomes the limitations of the structure functions of Ref. [109] in describing the region of $Q^2 \lesssim 0.2$ GeV^2. The remaining discrepancies between our theoretical calculations and experiments are most likely due to the in-medium broadening of the $\Delta(1232)$ [110], which is missing in the present version of the DCC model. The MEC may also need to be refined by, for example, carefully analyzing the $\gamma d \to pn$ reaction, as has been done in Ref. [30]. Finally, the aforementioned missing interference between one-and two-body
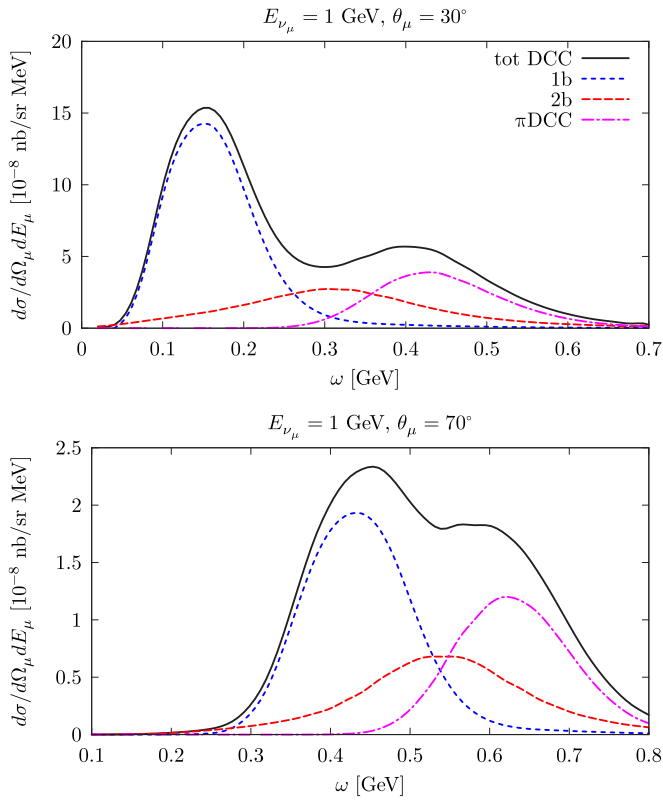
FIG. 12. Double-differential cross section for the $\nu_\mu + {}^{12}C \rightarrow \mu^- + X$ process at $E_\nu = 1$ GeV, $\theta_\mu = 30°$ (upper panel), and $E_\nu = 1$ GeV, $\theta_\mu = 70°$ (lower panel). The different curves are the same as in Fig. 11.

currents, together with a full account of FSI in two-nucleon knockout and pion-production processes are all needed to further improve the agreement with experiment. All these points will be addressed in future work.

The results obtained for the double-differential CC ν_μ-${}^{12}C$ scattering cross sections are shown in Fig. 12 for $E_\nu = 1$ GeV, $\theta_\mu = 30°$ (upper panel), and $E_\nu = 1$ GeV, $\theta_\mu = 70°$ (lower panel). The calculations have been carried out within the same framework employed in the electromagnetic case. The only additional ingredients are the axial terms in the current operators and in the π-production amplitudes. Consistently with the results of Fig. 11 and with Ref. [27], the relative strength of the MEC contribution increases with the scattering angle, reflecting the primarily transverse nature of this term even when axial terms are present. To the best of our knowledge, precise inclusive neutrino double-differential cross section data covering the $\Delta(1232)$ region are not available, yet. Comparing our theoretical calculations with such data requires a convolution with the neutrino energy spectrum of the experiments. In this work, primarily aimed at demonstrating the possibility of including relativistic one- and two-body current together with reliable pion-production amplitudes, we refrain from presenting flux-folded results. To this aim, a more sophisticated treatment of FSI, for both two-nucleon knockout and pion-production processes is required.

V. CONCLUSIONS

We have carried out calculations of electron- and neutrino-scattering off ${}^{12}C$ in the broad kinematical region of interest for current and planned neutrino-oscillation experiments. The EFS has allowed us to combine a realistic description of nuclear dynamics in both the initial target state and the spectator system—achieved by employing a SF computed within the CBF theory [24]—with an interaction vertex, suitable to include different reaction mechanisms. The QE and "dip" regions are investigated by including one- and two-body currents. In-medium modification of the Δ propagator is accounted for by a phenomenological potential derived within BHF [51–54]. The consequent reduction of the MEC strength is less important than the one resulting from the ad hoc prescription of disregarding the imaginary part of the Δ propagator [82,85,86]. The elementary amplitudes relevant for pion-production processes are obtained within the ANL-Osaka DCC model [41–43], which contains about 20 nucleon resonances, can be reliably utilized up to an invariant mass of $W \leqslant 2.1$ GeV. Their numerical implementation has required a further development of our highly-parallel Metropolis Monte Carlo integration technique.

To quantitatively assess the role of realistic hole-SF and FSI effects, we first computed the electron-${}^{12}C$ double-differential cross sections for incoming energy $E_e = 730$ MeV and scattering angle $\theta_e = 37°$. An accurate treatment of nuclear dynamics in both the initial and final states is required to reproduce experimental data. In particular, both the GRFG model and the simplest version of the PWIA—in which the excitation energies of the spectator system are assumed to be constant—noticeably overestimate the strength of the quasielastic peak. We have carried out calculations for the electron-${}^{12}C$ cross sections for three additional kinematical setups, corresponding to incoming energies $E_e = 620$ MeV, $E_e = 960$ MeV, $E_e = 1650$ MeV and scattering angles $\theta_e = 60°$, $\theta_e = 37.5°$, and $\theta_e = 11.95°$, respectively. In all cases, we observe an overall good agreement between data and our full theoretical model. Analyzing the separate contributions of the different elementary reaction mechanisms it clearly emerges that including the ANL-Osaka DCC pion-production amplitudes is crucial to reproduce experimental data in the resonance region. Consistently with Ref. [27], MEC are of primarily transverse nature and are needed to fill the missing strength between the Δ and the QE peaks. There are three main missing ingredients in our framework that are responsible for the relatively small discrepancies with experimental data. In this work we have neglected the interference between one- and two-body currents, which has been proven to enhance the QE peak of the transverse response function [25,60]. In addition, the treatment of FSI in two-nucleon emission processes is not as accurate as in the one-nucleon knockout case, whereas for real-pion production they are neglected altogether. Finally, at variance with the MEC, the ANL-Osaka DCC amplitudes do not encompass any in-medium modifications of the $\Delta(1232)$. More generally, it has to be noted that the MEC employed in this work were derived in Ref. [82] based on the HNV weak pion-production model [83]. As found in Ref. [111], the bulk of the ANL-Osaka DCC

model predictions for electro-production of pions in the Δ region could be reproduced by the simpler HNV model. A reasonable agreement is also found for the total cross section of CC processes. Nevertheless, efforts to employ MEC that are consistent with the ANL-Osaka DCC amplitudes are ongoing.

Within the same framework adopted to study inclusive electromagnetic scattering, we have carried out calculations of the double-differential CC ν_μ-^{12}C scattering cross sections for $E_\nu = 1\,\text{GeV}$, $\theta_\mu = 30°$ and $E_\nu = 1\,\text{GeV}$, $\theta_\mu = 70°$. As expected, real-pion emission provides significant excess strength in the Δ peak, while MEC primarily contribute in the dip region. In view of the above-mentioned limitations, we refrain from computing the flux-folded differential cross sections, which could be readily compared to experimental data. Work in this direction is underway, and, together with a further extension of the factorization scheme to account for two-pion emission processes will be the subject of future works.

[1] O. Benhar, P. Huber, C. Mariani, and D. Meloni, Phys. Rep. **700**, 1 (2017).

[2] T. Katori and M. Martini, J. Phys. G **45**, 013001 (2018).

[3] L. Alvarez-Ruso *et al.*, Prog. Part. Nucl. Phys. **100**, 1 (2018).

[4] A. A. Aguilar-Arevalo *et al.* (MiniBooNE Collaboration), Phys. Rev. Lett. **100**, 032301 (2008).

[5] A. A. Aguilar-Arevalo *et al.* (MiniBooNE Collaboration), Phys. Rev. D **81**, 092005 (2010).

[6] T. Leitner, O. Buss, L. Alvarez-Ruso, and U. Mosel, Phys. Rev. C **79**, 034601 (2009).

[7] O. Benhar, P. Coletti, and D. Meloni, Phys. Rev. Lett. **105**, 132301 (2010).

[8] M. Martini, M. Ericson, G. Chanfray, and J. Marteau, Phys. Rev. C **81**, 045502 (2010).

[9] M. Martini, M. Ericson, and G. Chanfray, Phys. Rev. C **84**, 055502 (2011).

[10] J. Nieves, I. Ruiz Simo, and M. J. Vicente Vacas, Phys. Rev. C **83**, 045501 (2011).

[11] J. Nieves, I. Ruiz Simo, and M. J. Vicente Vacas, Phys. Lett. B **707**, 72 (2012).

[12] G. D. Megias *et al.*, Phys. Rev. D **91**, 073004 (2015).

[13] R. Gonzaláz-Jiménez, G. D. Megias, M. B. Barbaro, J. A. Caballero, and T. W. Donnelly, Phys. Rev. C **90**, 035501 (2014).

[14] V. Pandey, N. Jachowicz, T. Van Cuyck, J. Ryckebusch, and M. Martini, Phys. Rev. C **92**, 024606 (2015).

[15] J. Carlson, S. Gandolfi, F. Pederiva, S. C. Pieper, R. Schiavilla, K. E. Schmidt, and R. B. Wiringa, Rev. Mod. Phys. **87**, 1067 (2015).

[16] A. Lovato, S. Gandolfi, J. Carlson, S. C. Pieper, and R. Schiavilla, Phys. Rev. Lett. **112**, 182502 (2014).

[17] A. Lovato, S. Gandolfi, J. Carlson, E. Lusk, S. C. Pieper, and R. Schiavilla, Phys. Rev. C **97**, 022502 (2018).

[18] Tokai to Kamioka, http://t2k-experiment.org/.

[19] Micro Booster Neutrino Experiment, https://microboone.fnal.gov.

[20] Main Injector Experiment for ν-A, https://minerva.fnal.gov.

[21] NuMI Off-axis ν_e Appearance, https://novaexperiment.fnal.gov.

[22] The Deep Underground Neutrino Experiment, http://www.dunescience.org.

[23] L. Madeira, A. Lovato, F. Pederiva, and K. E. Schmidt, Phys. Rev. C **98**, 034005 (2018).

[24] O. Benhar, D. Day, and I. Sick, Rev. Mod. Phys. **80**, 189 (2008).

[25] O. Benhar, A. Lovato, and N. Rocco, Phys. Rev. C **92**, 024602 (2015).

[26] N. Rocco, A. Lovato, and O. Benhar, Phys. Rev. Lett. **116**, 192501 (2016).

[27] N. Rocco, C. Barbieri, O. Benhar, A. De Pace, and A. Lovato, Phys. Rev. C **99**, 025502 (2019).

[28] I. Blomqvist and J. M. Laget, Nucl. Phys. A **280**, 405 (1977).

[29] J. H. Koch and N. Ohtsuka, Nucl. Phys. A **435**, 765 (1985).

[30] C. R. Chen and T.-S. H. Lee, Phys. Rev. C **38**, 2187 (1988).

[31] T.-S. H. Lee and R. P. Redwine, Annu. Rev. Nucl. Part. Sci. **52**, 23 (2002).

[32] M. Hirata, F. Lenz, and K. Yazaki, Ann. Phys. (NY) **108**, 116 (1977).

[33] M. Hirata, J. H. Koch, E. J. Moniz, and F. Lenz, Ann. Phys. (NY) **120**, 205 (1979).

[34] Y. Horikawa, M. Thies, and F. Lenz, Nucl. Phys. A **345**, 386 (1980).

[35] B. Szczerbinska, T. Sato, K. Kubodera, and T.-S. H. Lee, Phys. Lett. B **649**, 132 (2007).

[36] T. Sato and T.-S. H. Lee, Phys. Rev. C **54**, 2660 (1996).

[37] T. Sato and T.-S. H. Lee, Phys. Rev. C **63**, 055201 (2001).

[38] O. Benhar, A. Fabrocini, and S. Fantoni, Nucl. Phys. A **505**, 267 (1989).

[39] O. Benhar, A. Fabrocini, S. Fantoni, and I. Sick, Nucl. Phys. A **579**, 493 (1994).

[40] T. Sato, D. Uno, and T.-S. H. Lee, Phys. Rev. C **67**, 065201 (2003).

[41] H. Kamano, S. X. Nakamura, T.-S. H. Lee, and T. Sato, Phys. Rev. C **88**, 035209 (2013).

[42] S. X. Nakamura, H. Kamano, and T. Sato, Phys. Rev. D **92**, 074024 (2015).

[43] H. Kamano, S. X. Nakamura, T.-S. H. Lee, and T. Sato, Phys. Rev. C **94**, 015201 (2016).

[44] K. Nakamura and P. D. Group, J. Phys. G: Nucl. Part. Phys. **37**, 075021 (2010).

[45] E. Vagnoni, O. Benhar, and D. Meloni, Phys. Rev. Lett. **118**, 142502 (2017).

[46] E. A. Paschos, J.-Y. Yu, and M. Sakuda, Phys. Rev. D **69**, 014013 (2004).

[47] O. Lalakulich and E. A. Paschos, Phys. Rev. D **71**, 074003 (2005).

[48] O. Lalakulich, E. A. Paschos, and G. Piranishvili, Phys. Rev. D **74**, 014009 (2006).

[49] T.-S. H. Lee and K. Ohta, Phys. Rev. C **25**, 3043 (1982).

[50] T.-S. H. Lee, Phys. Rev. C **54**, 1350 (1996).

[51] T.-S. H. Lee, Phys. Rev. Lett. **50**, 1571 (1983).

[52] T.-S. H. Lee, Phys. Rev. C **29**, 195 (1984).

[53] T.-S. H. Lee and A. Matsuyama, Phys. Rev. C **32**, 516 (1985).

[54] T.-S. H. Lee and A. Matsuyama, Phys. Rev. C **36**, 1459 (1987).

[55] G. Shen, L. E. Marcucci, J. Carlson, S. Gandolfi, and R. Schiavilla, Phys. Rev. C **86**, 035503 (2012).

[56] O. Benhar and D. Meloni, Nucl. Phys. A **789**, 379 (2007).

[57] P. Herczeg, C. M. Hoffman, and H. V. Klapdor-Kleingrothaus, *Physics Beyond the Standard Model* (World Scientific, Singapore, 1999), pp. 1–802, https://www.worldscientific.com/doi/pdf/10.1142/9789814527514.

[58] S. Nakamura, T. Sato, S. Ando, T. S. Park, F. Myhrer, V. P. Gudkov, and K. Kubodera, Nucl. Phys. A **707**, 561 (2002).

[59] O. Benhar, D. Day, and I. Sick, arXiv:nucl-ex/0603032.

[60] A. Lovato, S. Gandolfi, J. Carlson, S. C. Pieper, and R. Schiavilla, Phys. Rev. Lett. **117**, 082501 (2016).

[61] J. Mougey, M. Bernheim, A. Bussiere, A. Gillibert, X. H. Phan, M. Priou, D. Royer, I. Sick, and G. J. Wagner, Nucl. Phys. A **262**, 461 (1976).

[62] S. Turck-Chièze, in *From Collective States to Quarks in Nuclei*, edited by H. Arenhövel and A. M. Saruis (Springer, Berlin/Heidelberg, 1981), pp. 251–257.

[63] D. Dutta *et al.* (JLab E91013 Collaboration), Phys. Rev. C **68**, 064603 (2003).

[64] R. B. Wiringa, V. G. J. Stoks, and R. Schiavilla, Phys. Rev. C **51**, 38 (1995).

[65] Argonne National Laboratory Theory Group, http://www.phy.anl.gov/theory/.

[66] A. M. Ankowski, O. Benhar, and M. Sakuda, Phys. Rev. D **91**, 033005 (2015).

[67] E. D. Cooper, S. Hama, B. C. Clark, and R. L. Mercer, Phys. Rev. C **47**, 297 (1993).

[68] O. Benhar, A. Fabrocini, S. Fantoni, G. A. Miller, V. R. Pandharipande, and I. Sick, Phys. Rev. C **44**, 2328 (1991).

[69] O. Benhar, Phys. Rev. C **87**, 024606 (2013).

[70] R. Gupta, Y.-C. Jang, H.-W. Lin, B. Yoon, and T. Bhattacharya, Phys. Rev. D **96**, 114503 (2017).

[71] A. S. Meyer, M. Betancourt, R. Gran, and R. J. Hill, Phys. Rev. D **93**, 113015 (2016).

[72] J. E. Sobczyk, N. Rocco, and J. Nieves, Phys. Rev. C **100**, 035501 (2019).

[73] A. Lovato, N. Rocco, and R. Schiavilla, Phys. Rev. C **100**, 035502 (2019).

[74] L. E. Marcucci, M. Viviani, R. Schiavilla, A. Kievsky, and S. Rosati, Phys. Rev. C **72**, 014001 (2005).

[75] M. J. Dekker, P. J. Brussaard, and J. A. Tjon, Phys. Lett. B **266**, 249 (1991).

[76] R. B. Wiringa, R. Schiavilla, S. C. Pieper, and J. Carlson, Phys. Rev. C **89**, 024305 (2014).

[77] R. Weiss, B. Bazak, and N. Barnea, Phys. Rev. C **92**, 054311 (2015).

[78] R. Weiss, I. Korover, E. Piasetzky, O. Hen, and N. Barnea, Phys. Lett. B **791**, 242 (2019).

[79] D. Lonardoni, S. Gandolfi, X. B. Wang, and J. Carlson, Phys. Rev. C **98**, 014322 (2018).

[80] L. L. Frankfurt and M. I. Strikman, Phys. Rep. **160**, 235 (1988).

[81] A. Fabrocini, Phys. Rev. C **55**, 338 (1997).

[82] I. Ruiz Simo, J. E. Amaro, M. B. Barbaro, A. De Pace, J. A. Caballero, and T. W. Donnelly, J. Phys. G **44**, 065105 (2017).

[83] E. Hernandez, J. Nieves, and M. Valverde, Phys. Rev. D **76**, 033005 (2007).

[84] M. J. Dekker, P. J. Brussaard, and J. A. Tjon, Phys. Rev. C **49**, 2650 (1994).

[85] A. De Pace, M. Nardi, W. M. Alberico, T. W. Donnelly, and A. Molinari, Nucl. Phys. A **726**, 303 (2003).

[86] A. V. Butkevich and S. V. Luchuk, Phys. Rev. C **97**, 045502 (2018).

[87] K. Joo *et al.* (CLAS Collaboration), Phys. Rev. Lett. **88**, 122001 (2002).

[88] M. Ungaro *et al.* (CLAS Collaboration), Phys. Rev. Lett. **97**, 112003 (2006).

[89] H. Egiyan *et al.* (CLAS Collaboration), Phys. Rev. C **73**, 025204 (2006).

[90] K. Park *et al.* (CLAS Collaboration), Phys. Rev. C **77**, 015208 (2008).

[91] K. Park *et al.* (CLAS Collaboration), Phys. Rev. C **91**, 045203 (2015).

[92] M. Kobayashi, T. Sato, and H. Ohtsubo, Prog. Theor. Phys. **98**, 927 (1997).

[93] P. Rodrigues, C. Wilkinson, and K. McFarland, Eur. Phys. J. C **76**, 474 (2016).

[94] S. J. Barish *et al.*, Phys. Rev. D **19**, 2521 (1979).

[95] T. Kitagaki *et al.*, Phys. Rev. D **34**, 2554 (1986).

[96] S. X. Nakamura *et al.*, Rep. Prog. Phys. **80**, 056301 (2017).

[97] D. Rein and L. M. Sehgal, Ann. Phys. (NY) **133**, 79 (1981).

[98] S. X. Nakamura, H. Kamano, and T. Ishikawa, Phys. Rev. C **96**, 042201 (2017).

[99] S. X. Nakamura, Phys. Rev. C **98**, 042201 (2018).

[100] S. X. Nakamura, H. Kamano, and T. Sato, Phys. Rev. D **99**, 031301 (2019).

[101] S. X. Nakamura, H. Kamano, T.-S. H. Lee, and T. Sato, arXiv:1804.04757.

[102] W. N. Polyzou and C. Elster, J. Phys. G **41**, 094006 (2014).

[103] W. N. Polyzou, W. Glöckle, and H. Witała, *Proceedings of the Theory and Experiment for Hadrons on the Light-Front (Light Cone 2014): Raleigh, North Carolina, USA, May 26–30, 2014* [Few Body Syst. **56**, 395 (2015)].

[104] W. N. Polyzou, private communication.

[105] C. Colle, W. Cosyn, and J. Ryckebusch, Phys. Rev. C **93**, 034608 (2016).

[106] E. Hernández, J. Nieves, and M. J. Vicente Vacas, Phys. Rev. D **87**, 113009 (2013).

[107] O. Lalakulich and U. Mosel, Phys. Rev. C **87**, 014602 (2013).

[108] J. E. Sobczyk, N. Rocco, A. Lovato, and J. Nieves, Phys. Rev. C **97**, 035506 (2018).

[109] A. Bodek and J. L. Ritchie, Phys. Rev. D **23**, 1070 (1981).

[110] S. X. Nakamura, T. Sato, T.-S. H. Lee, B. Szczerbinska, and K. Kubodera, Phys. Rev. C **81**, 035502 (2010).

[111] J. E. Sobczyk, E. Hernández, S. X. Nakamura, J. Nieves, and T. Sato, Phys. Rev. D **98**, 073001 (2018).